Supporting Information

Colorimetric chemosensor for multiple targets, Cu^{2+}, CN$^-$ and S^{2-}

Ka Young Ryu, Jae Jun Lee, Jin Ah Kim, Dae Yul Park, Cheal Kim*

Department of Fine Chemistry and Department of Interdisciplinary Bio IT Materials, Seoul National University of Science and Technology, Seoul 139-743, Korea. Fax: +82-2-973-9149; Tel: +82-2-970-6693; E-mail: chealkim@seoultech.ac.kr
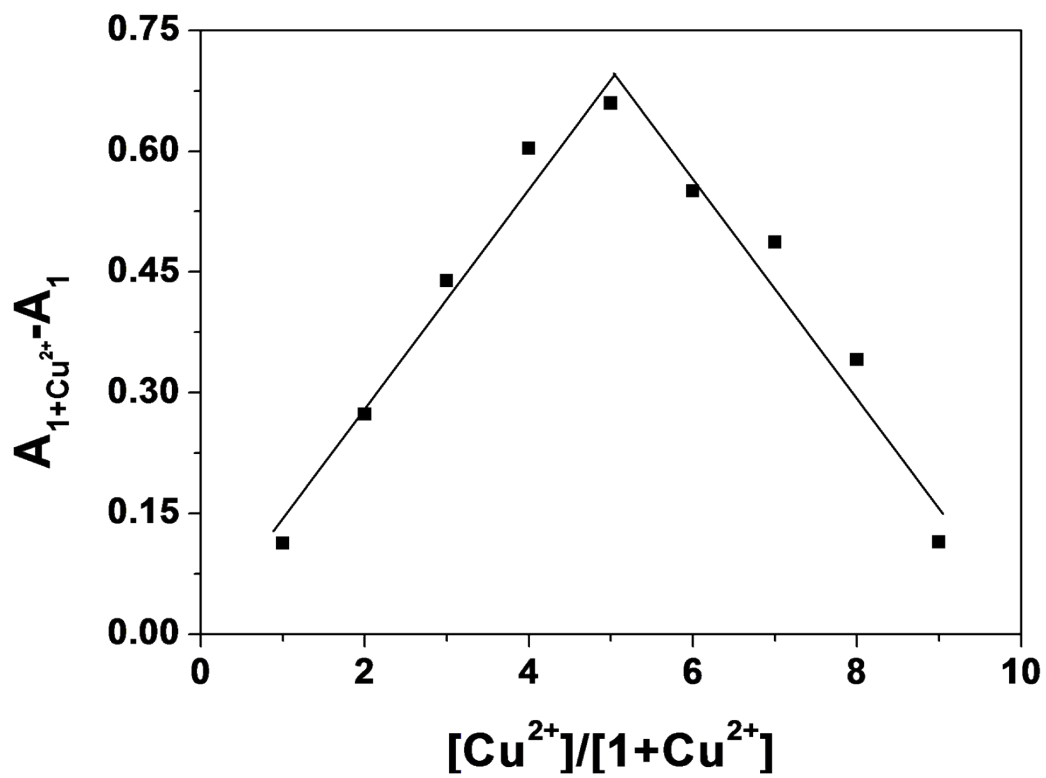
Figure S1. Job plot for the reaction of **1** with Cu^{2+}. Absorbance at 412 nm was plotted as a function of the molar ratio $[Cu^{2+}]/([1+Cu^{2+}])$. The total concentrations of Cu^{2+} with **1** were 100 μM.
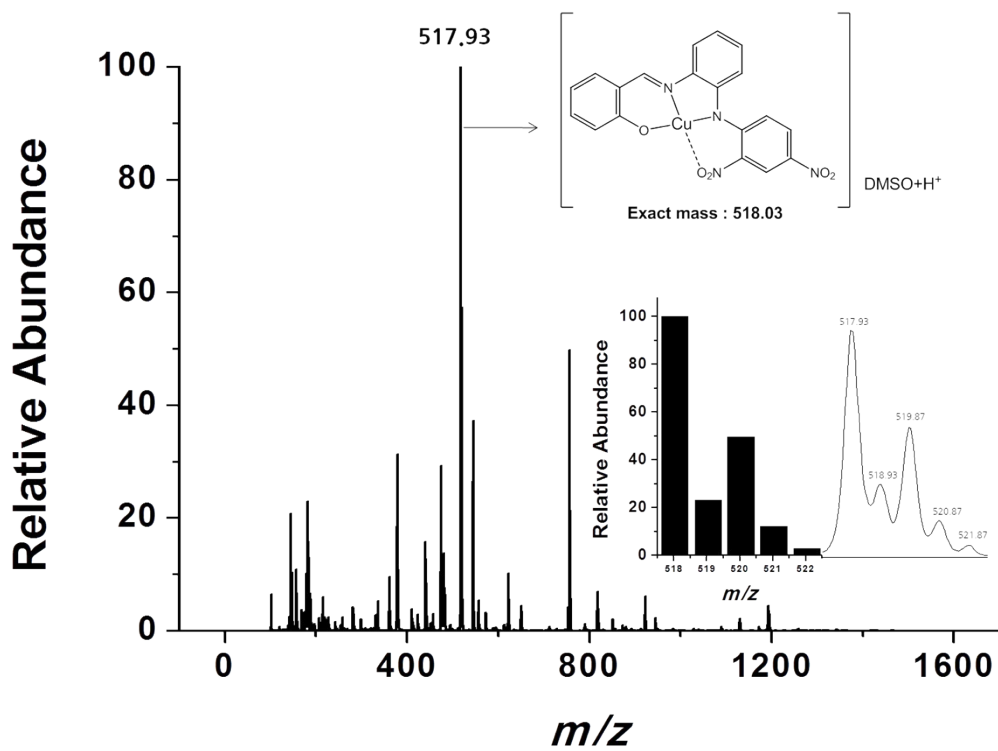
Figure S2. Positive-ion electrospray ionization mass spectrum of **1** (0.1 mM) upon addition of Cu^{2+} (0.1 mM).
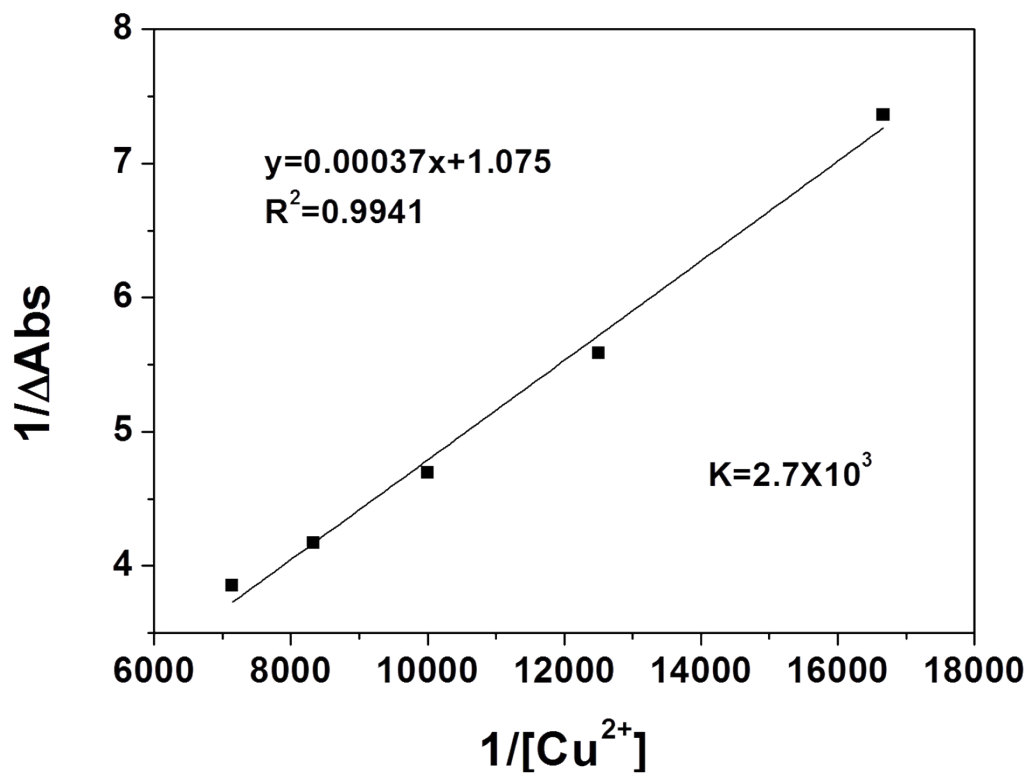
Figure S3. Benesi-Hidebrand equation plot (absorbance at 412 nm) of **1** (20 μM), assuming 1:1 stoichiometry for association between **1** and Cu^{2+}.
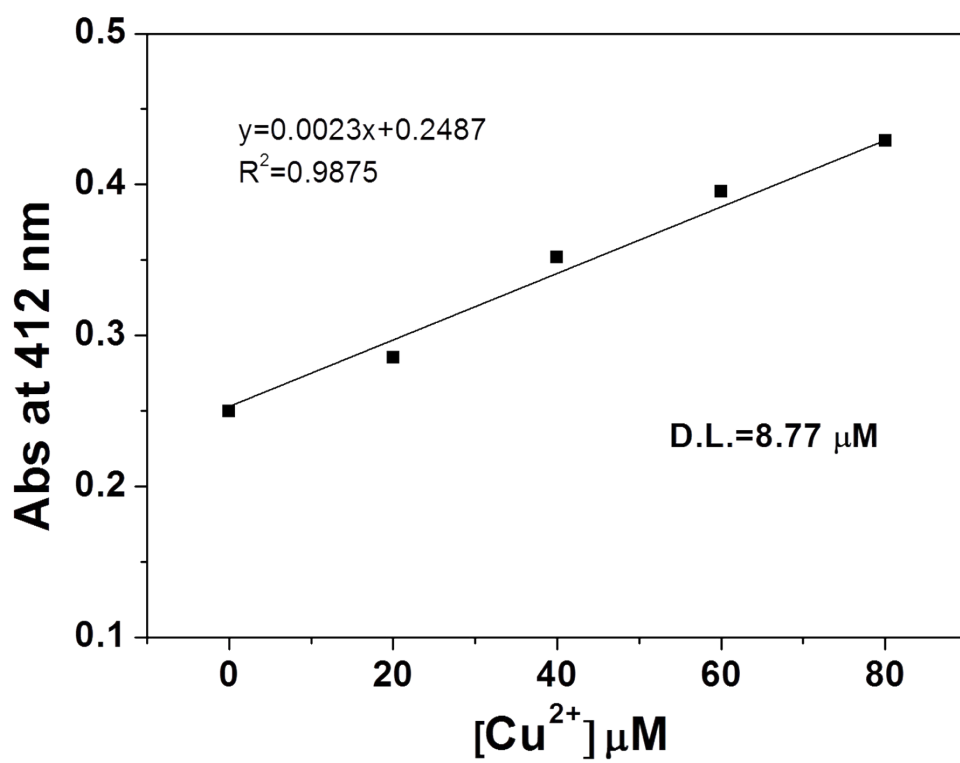
Figure S4. Determination of the detection limit based on change in the ratio (absorbance at 412 nm) of **1** (20 μM) with Cu^{2+}.
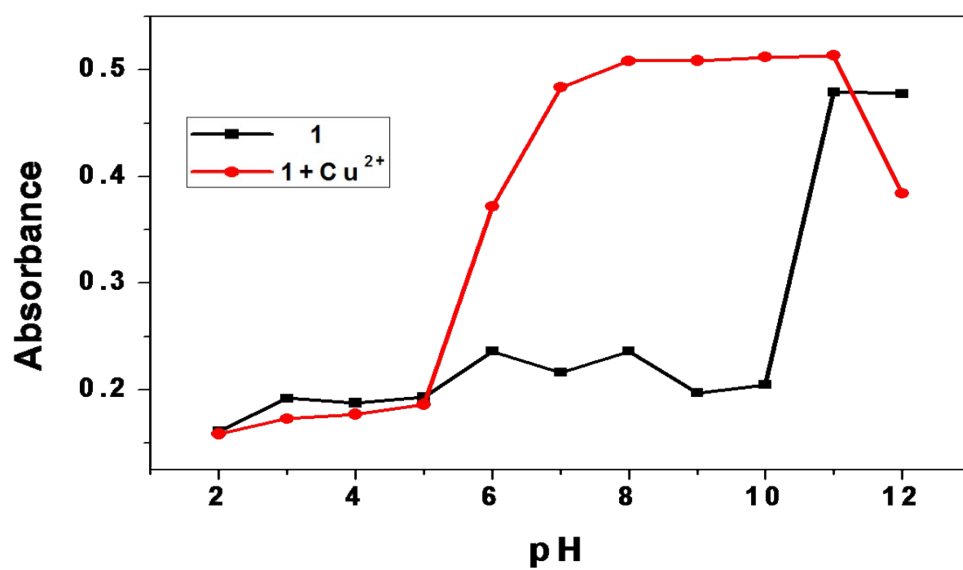
Figure S5. Absorbance of **1** and **1**-Cu^{2+} complex (412 nm) at different pH values (2-12) in a mixture of bis-tris buffer/DMSO (1:1, v/v).
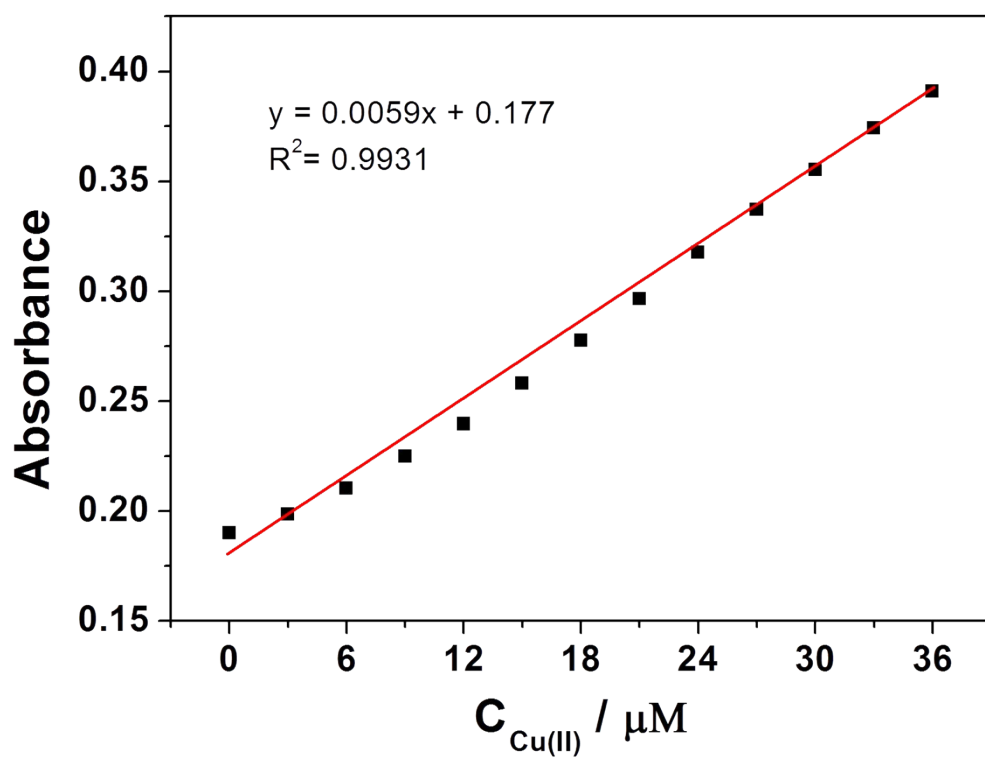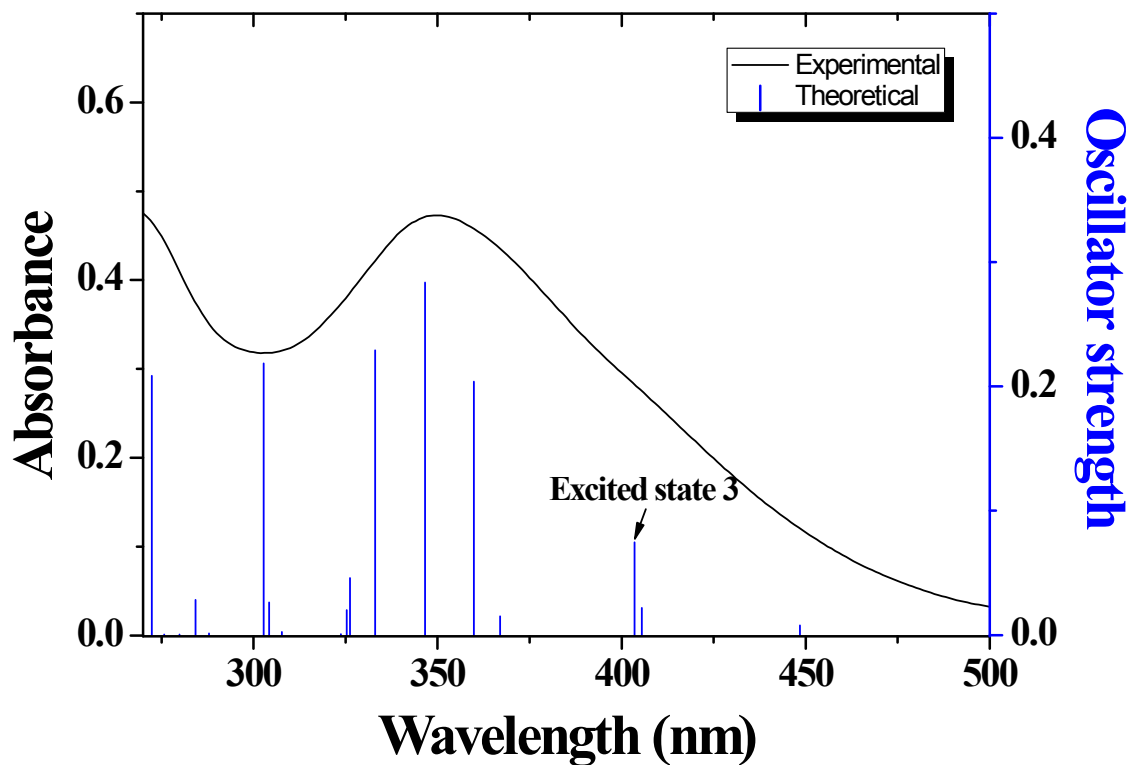
Figure S6. Absorption (at 412 nm) of **1** as a function of Cu(II) concentration. [**1**] = 20 µmol/L and [Cu(II)] = 0-36.0 µmol/L.

(a)

(b)

Excited State 3	Wavelength	Percent (%)	Main character	Oscillator strength
H - 1 → L	403.53 nm	93%	ICT	0.0747
H → L + 1		5%		

Figure S7. (a) The theoretical excitation energies and the experimental UV-vis spectrum of **1**. (b) The major electronic transition energies and molecular orbital contributions for **1** (H = HOMO and L = LUMO).

(a)
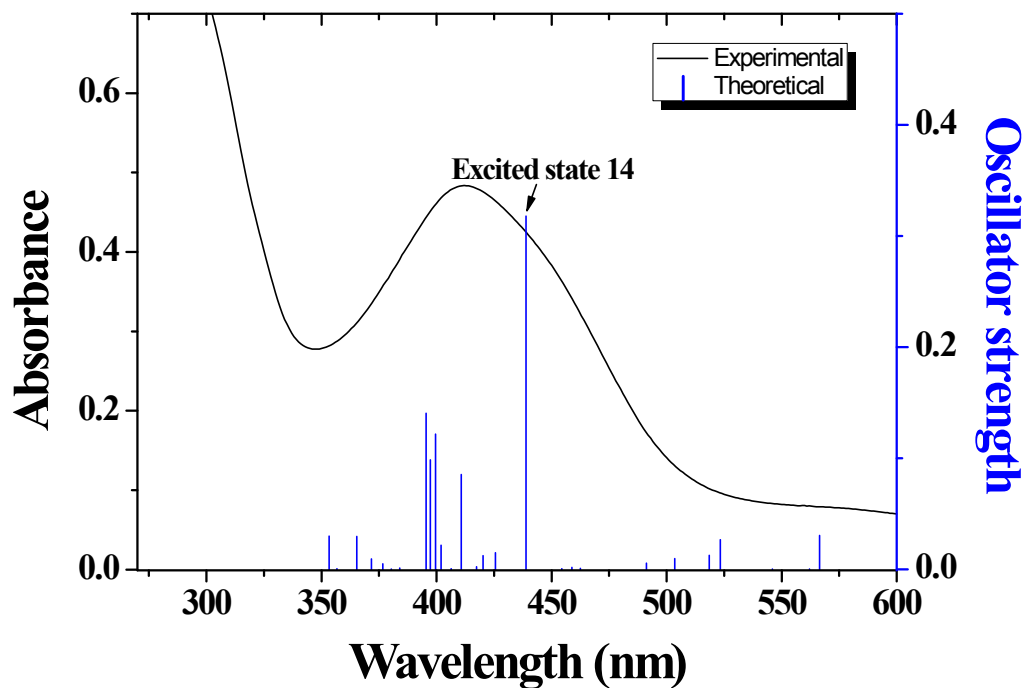
(b)

Excited State 14	Wavelength	Percent (%)	Main character	Oscillator strength
H → L+1 (α)	438.86 nm	45%	ICT	0.3178
H → L+2 (β)		40%	ICT	

Figure S8. (a) The theoretical excitation energies and the experimental UV-vis spectrum of **1**-Cu^{2+}. (b) The major electronic transition energies and molecular orbital contributions for **1**-Cu^{2+} (H = HOMO and L = LUMO / (α): α spin MO and (β): β spin MO).
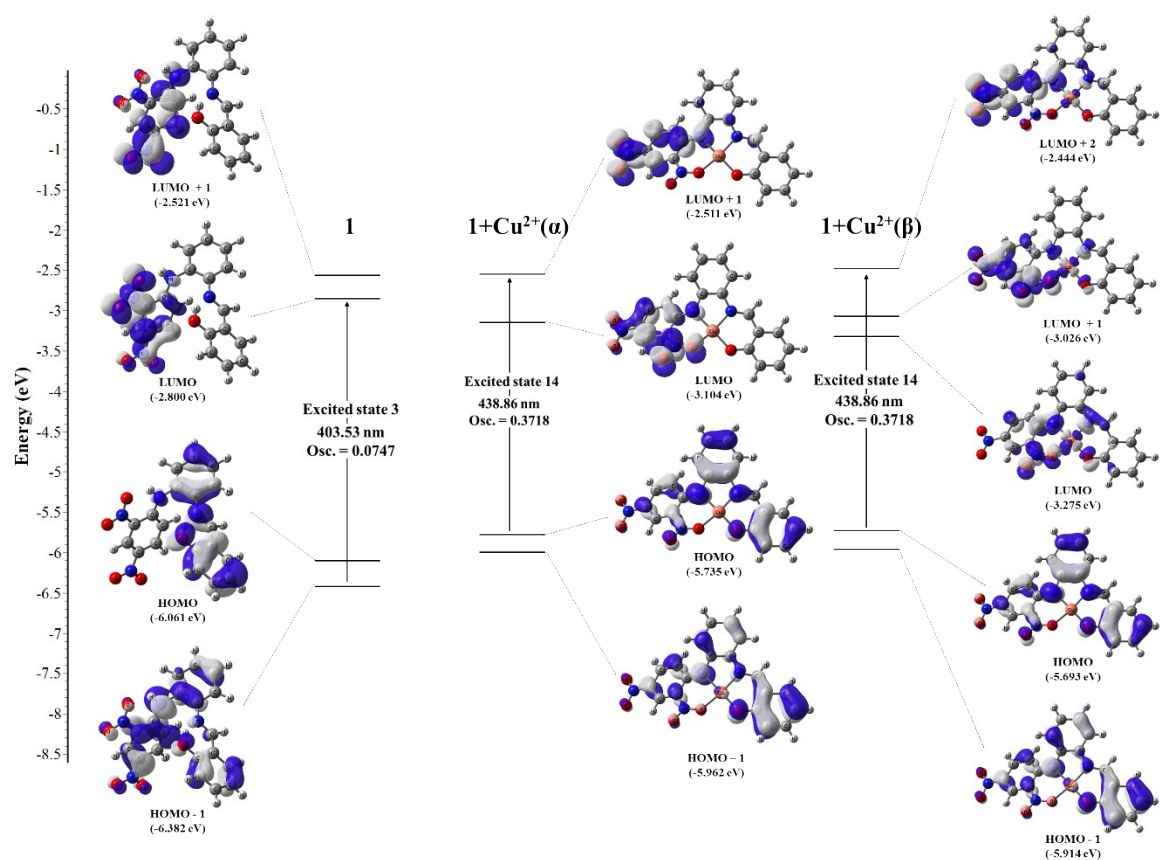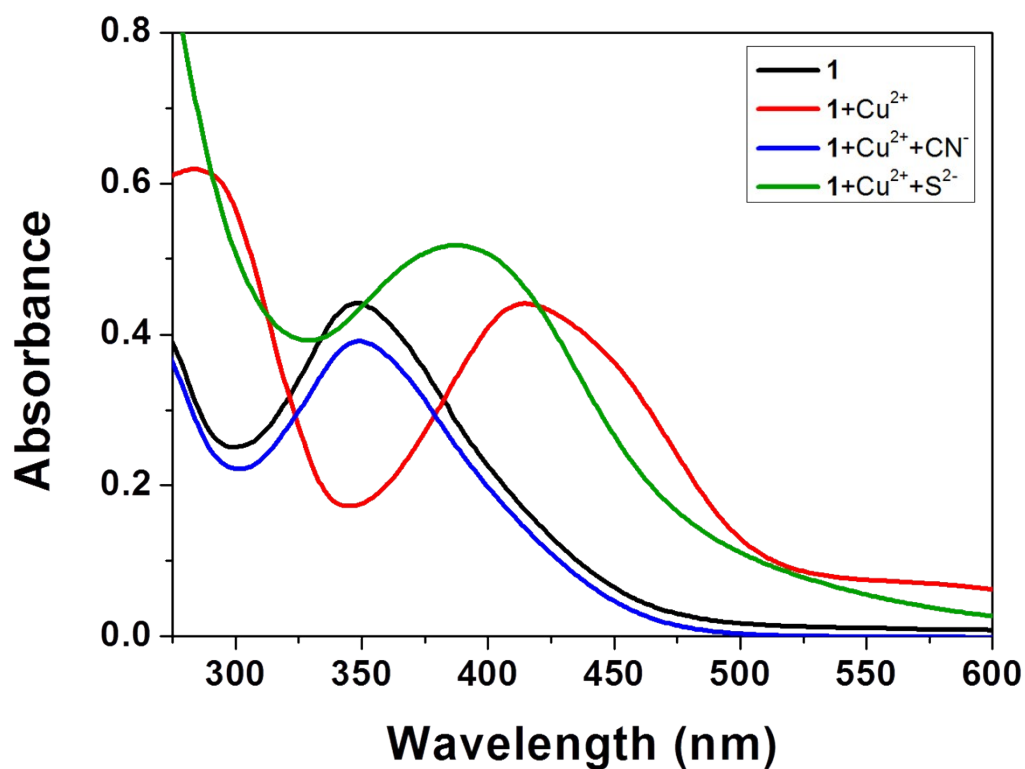
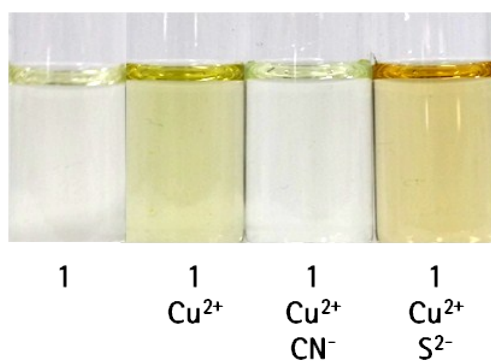**Figure S9.** Molecular orbital diagrams and excitation energies of **1** and **1**-Cu^{2+}.

(a)

(b)

Figure S10. (a) Absorption spectra and (b) color changes of **1**, **1**-Cu^{2+} complex, **1**-Cu^{2+} complex + CN^- and **1**-Cu^{2+} complex + S^{2-} in a mixture of bis-tris buffer/DMSO (1:1, v/v). Conditions; **1** = 20 μM, Cu^{2+} = 8 equiv, CN^- = 70 equiv, and S^{2-} = 80 equiv.
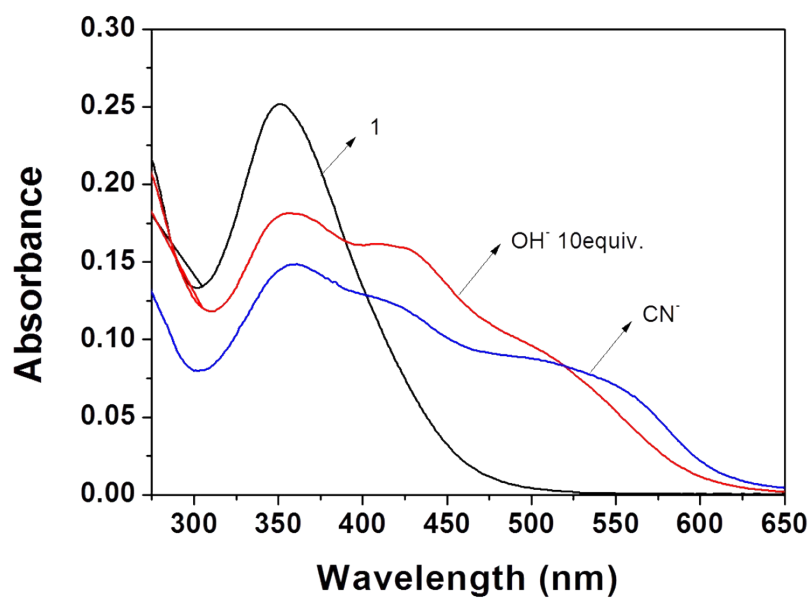
Figure S11. Absorption changes of **1** (10 μM) in the presence of TBAOH (10 equiv) and TBACN (100 equiv), respectively, in bis-tris buffer/DMSO (v/v=1:9).
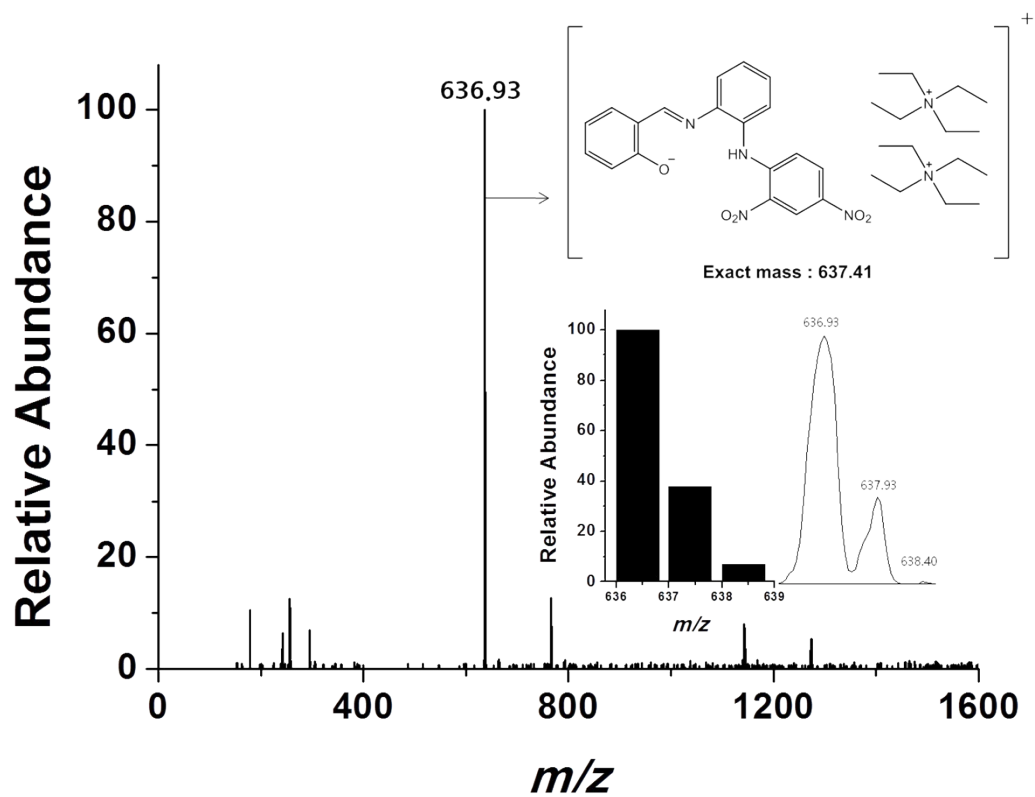
Figure S12. Positive-ion electrospray ionization mass spectrum of **1** (0.1 mM) upon addition of CN⁻ (0.1 mM).
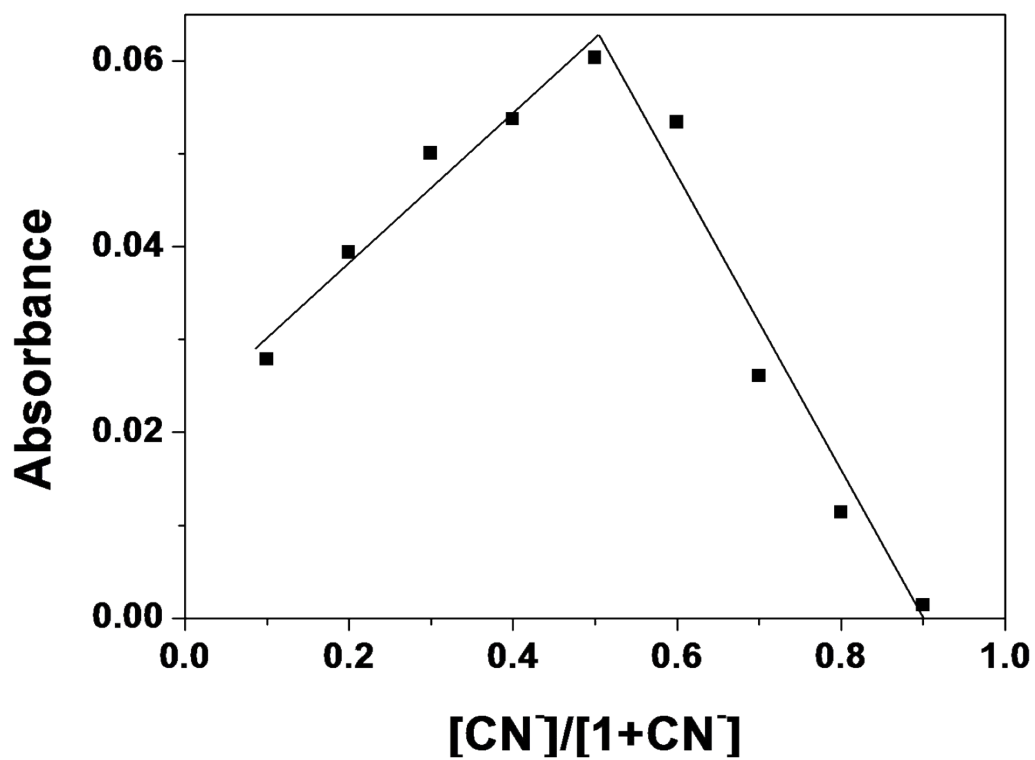
Figure S13. Job plot for the reaction of **1** with CN⁻. Absorbance at 500 nm was plotted as a function of the molar ratio [CN⁻]/[**1**+CN⁻]. The total concentrations of CN⁻ with receptor **1** were 100 μM.

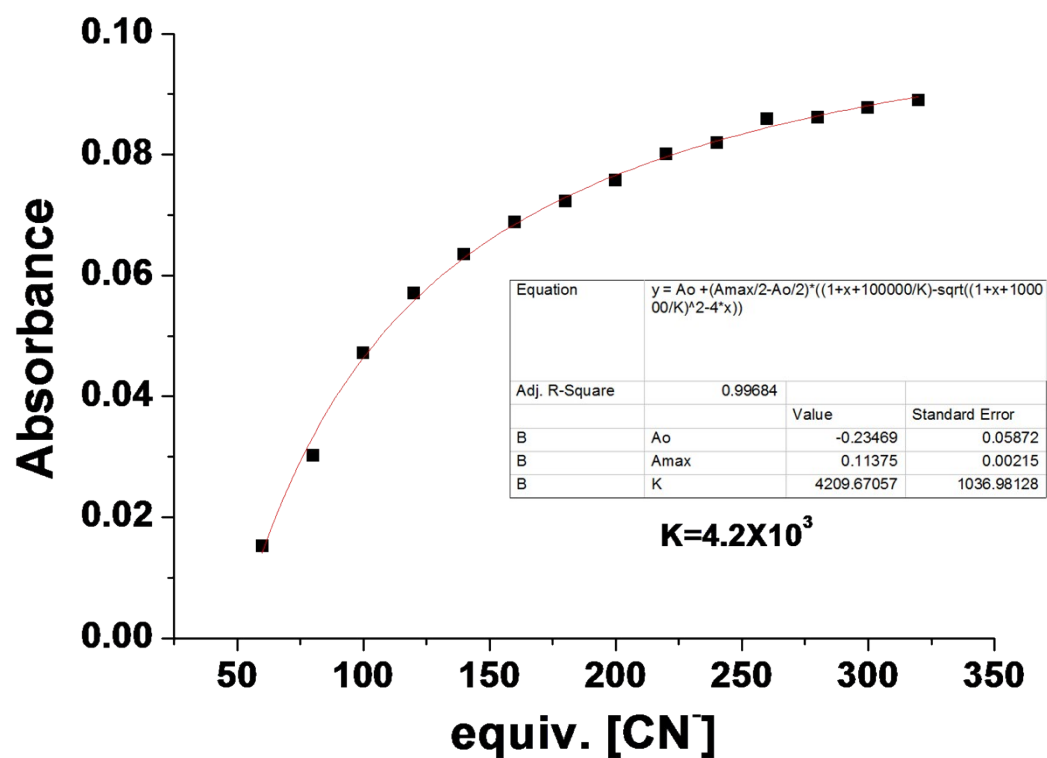| Equation	y = Ao +(Amax/2-Ao/2)*((1+x+100000/K)-sqrt((1+x+100000/K)^2-4*x))		
Adj. R-Square	0.99684		
		Value	Standard Error
B	Ao	-0.23469	0.05872
B	Amax	0.11375	0.00215
B	K	4209.67057	1036.98128

$K=4.2 \times 10^3$

Figure S14. UV-vis absorbance of **1** (10 μM) after addition of increasing different concentration of CN⁻. The red line is the non-linear fitting curve between **1** and CN⁻.
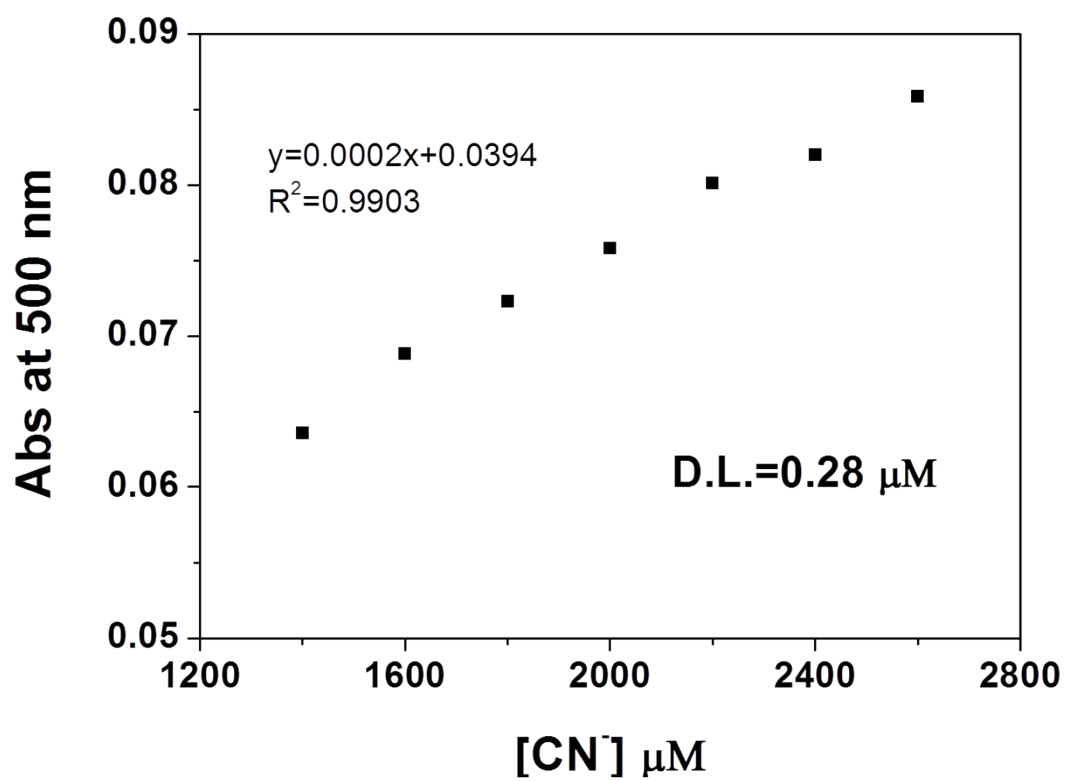
Figure S15. Determination of the detection limit based on change in the ratio (absorbance at 500 nm) of **1** (10 μM) with CN⁻.

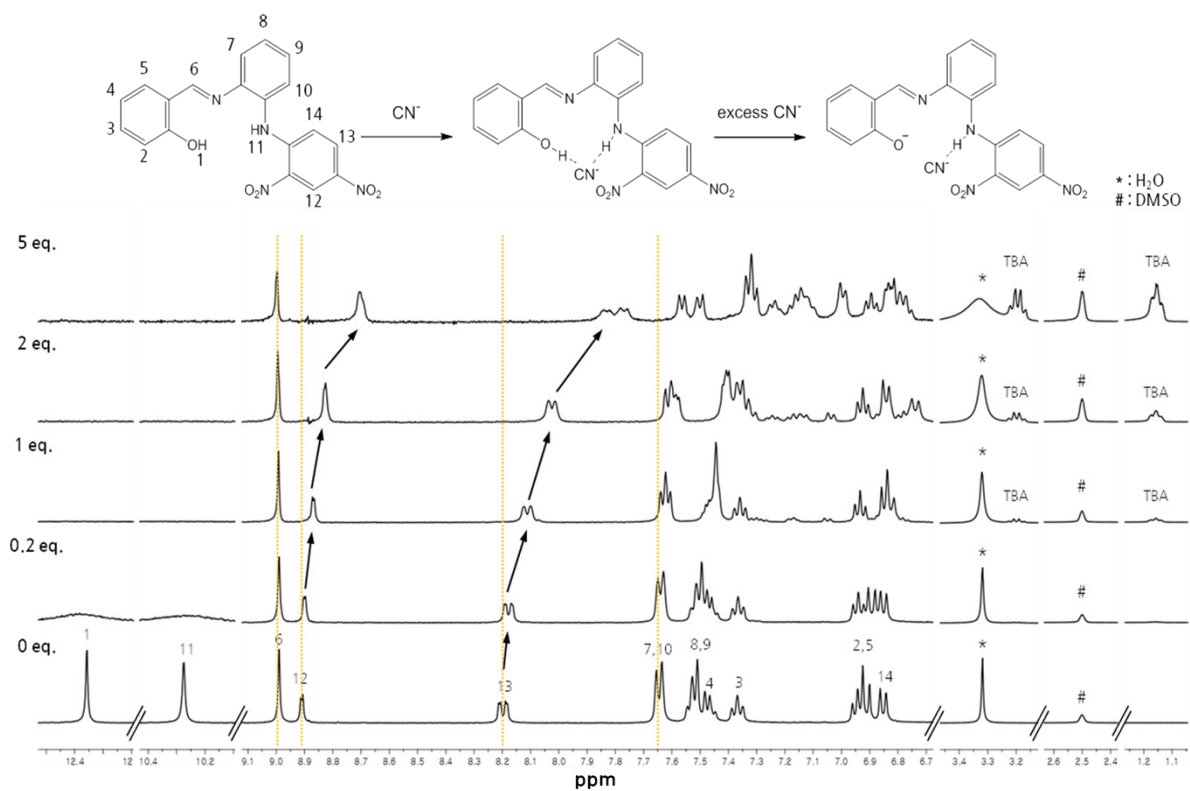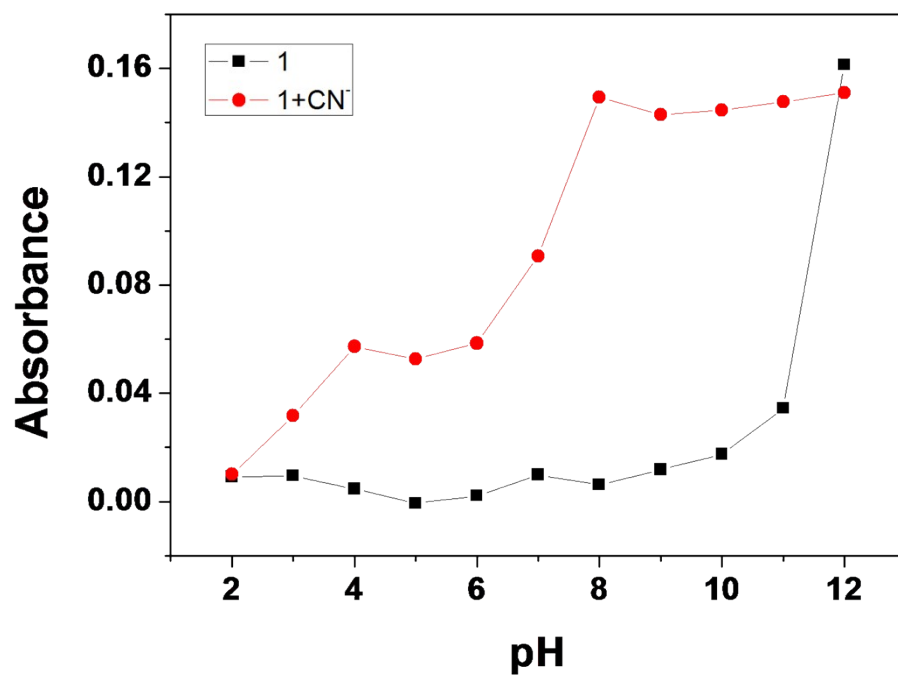**Figure S16.** ^{1}H NMR titration of receptor **1** with CN^{-}.
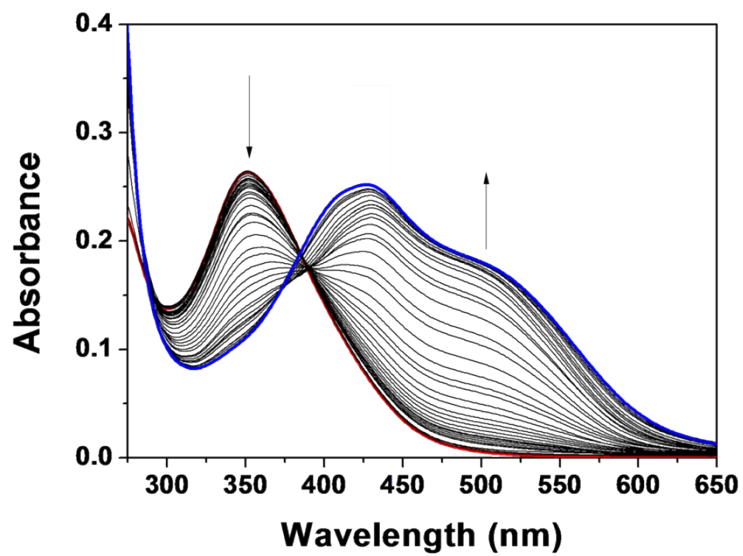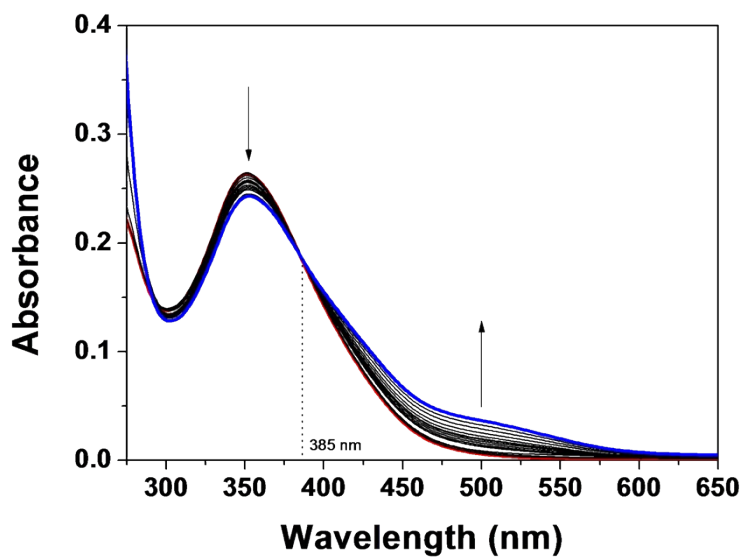
Figure S17. Absorbance of **1** and **1**-CN⁻ (500 nm) at different pH values (2-12) in a mixture of bis-tris buffer/DMSO (1:9, v/v).
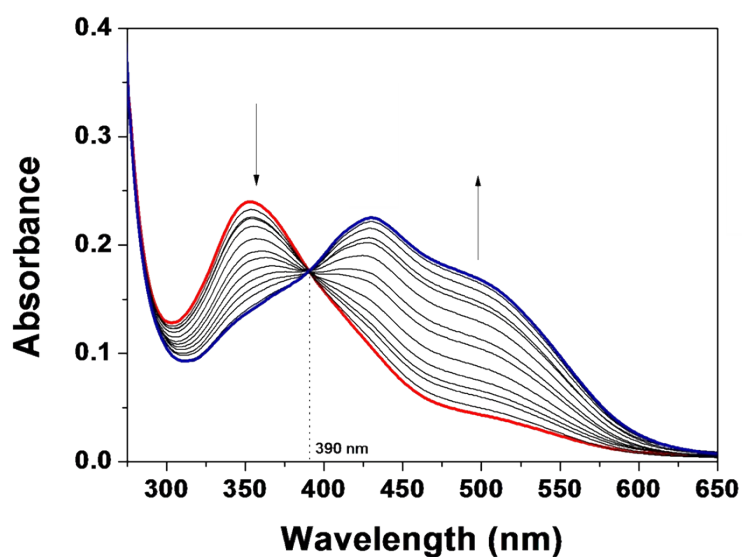
(a)

(b)
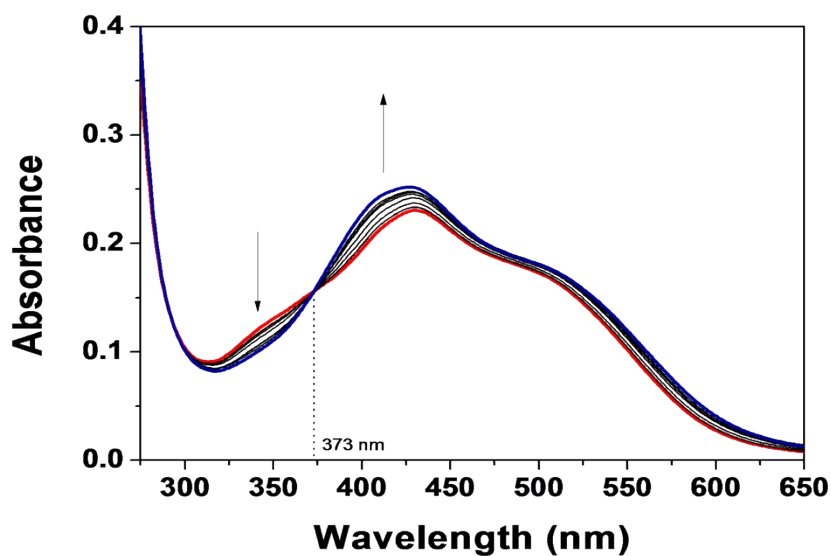

19

(c)

(d)

Figure S18. (a) Absorption spectral changes of **1** (10 μM) in the presence of different concentrations of S^{2-} (from 0 to 88 equiv) at room temperature. (b) Absorption spectral changes of **1** (10 μM), extracted from the range of 0-60 equiv of S^{2-} in (a). (c) Absorption spectral changes of **1** (10 μM), extracted from the range of 65-75 equiv of S^{2-} in (a). (d) Absorption spectral changes of **1** (10 μM), extracted from the range of 75-88 equiv of S^{2-} in
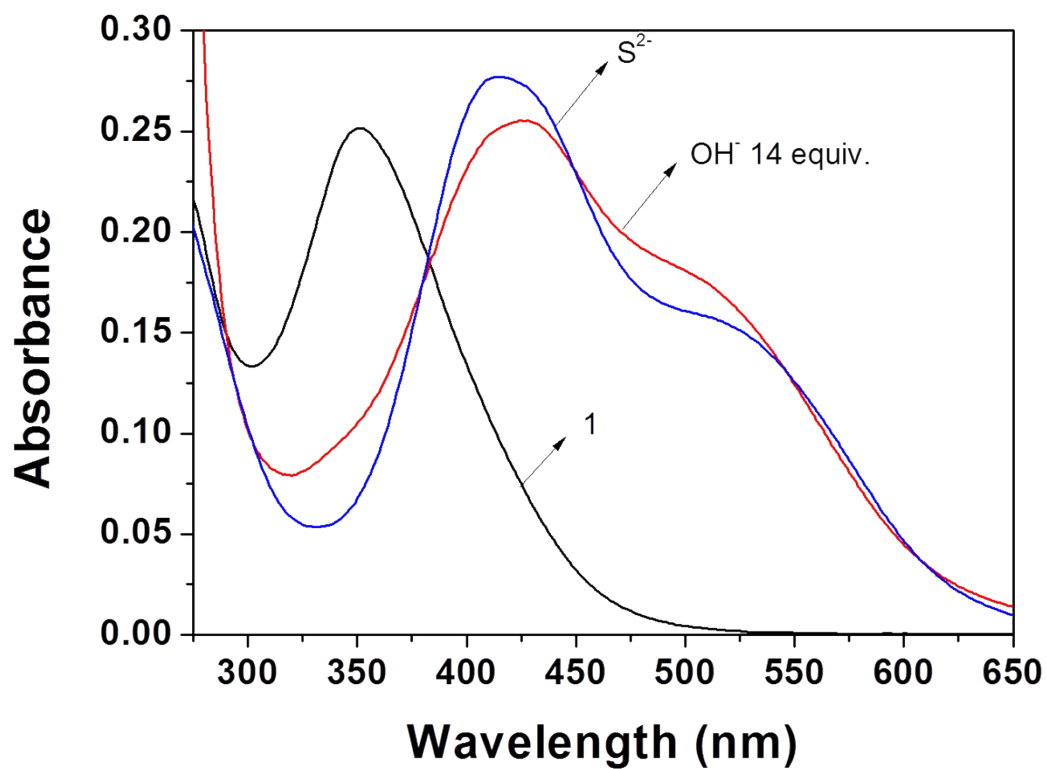
(a).

Figure S19. Absorption spectra of **1** (10 μM), and **1** (10 μM) in the presence of TBAOH (14 equiv) and Na$_2$S (88 equiv), respectively, in bis-tris buffer/DMSO (v/v=1:9).
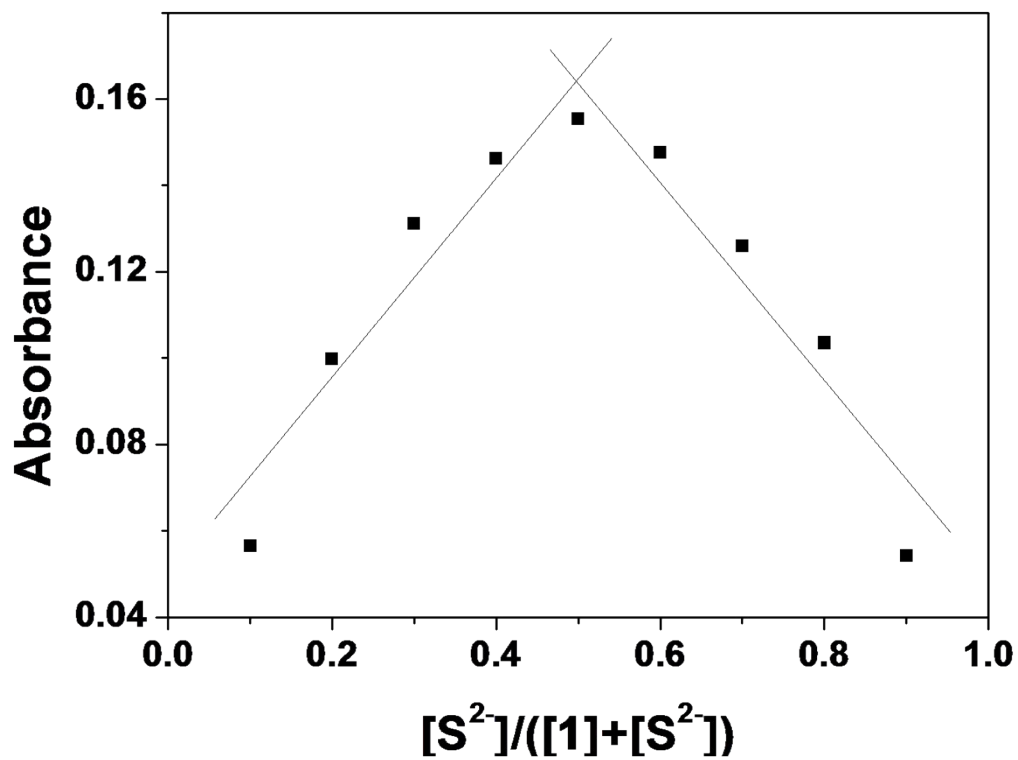
Figure S20. Job plot for the reaction of **1** with S^{2-}. Absorbance at 427 nm was plotted as a function of the molar ratio $[S^{2-}]/[\mathbf{1}+S^{2-}]$. The total concentrations of S^{2-} with receptor **1** were 100 μM.
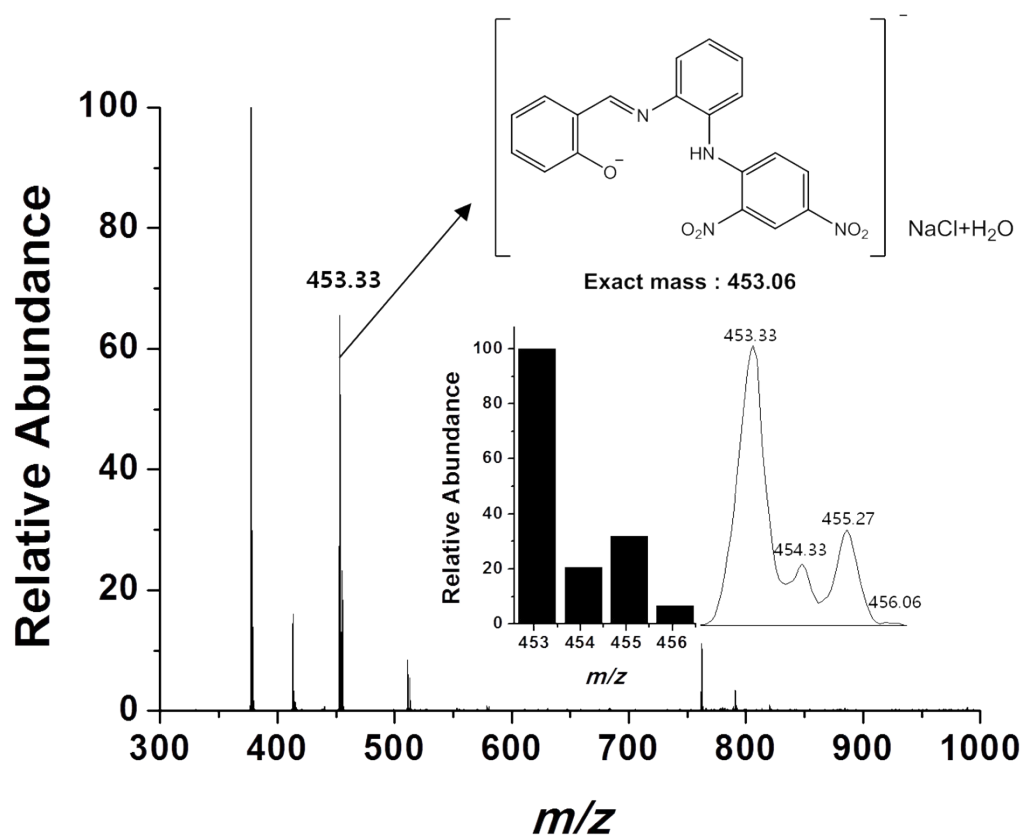
Figure S21. Negative-ion electrospray ionization mass spectrum of **1** (0.1 mM) upon addition of S^{2-} (0.1 mM).
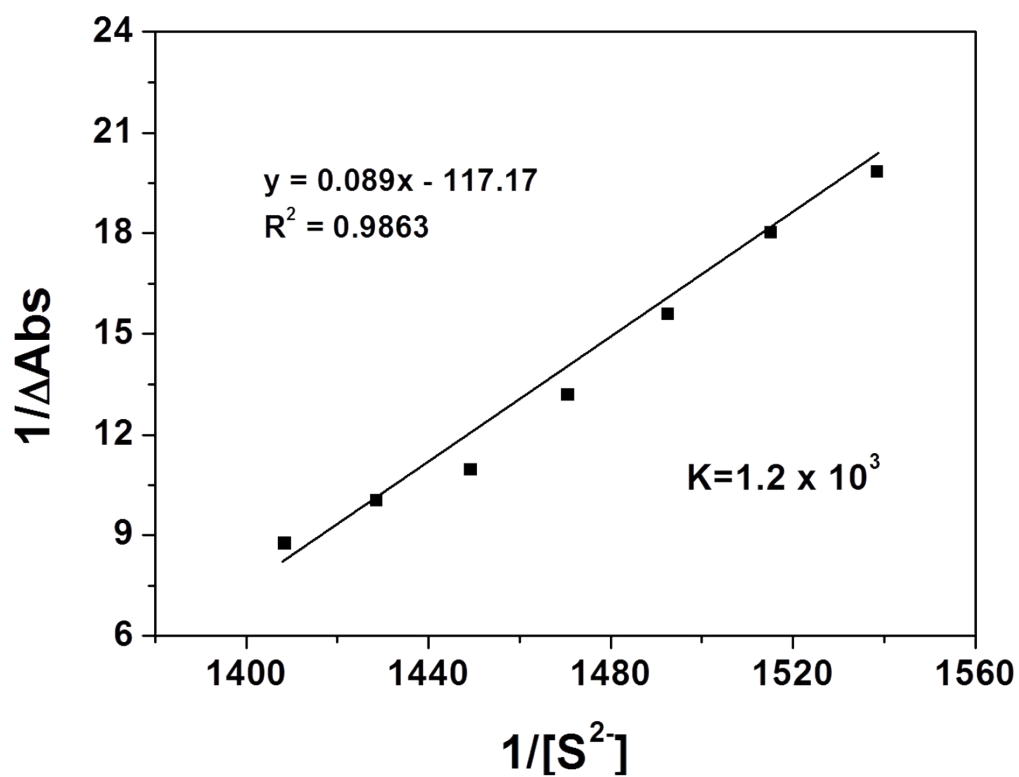
Figure S22. Benesi-Hidebrand equation plot (absorbance at 427 nm) of **1** (10μM), assuming 1:1 stoichiometry for association between **1** and S^{2-}.
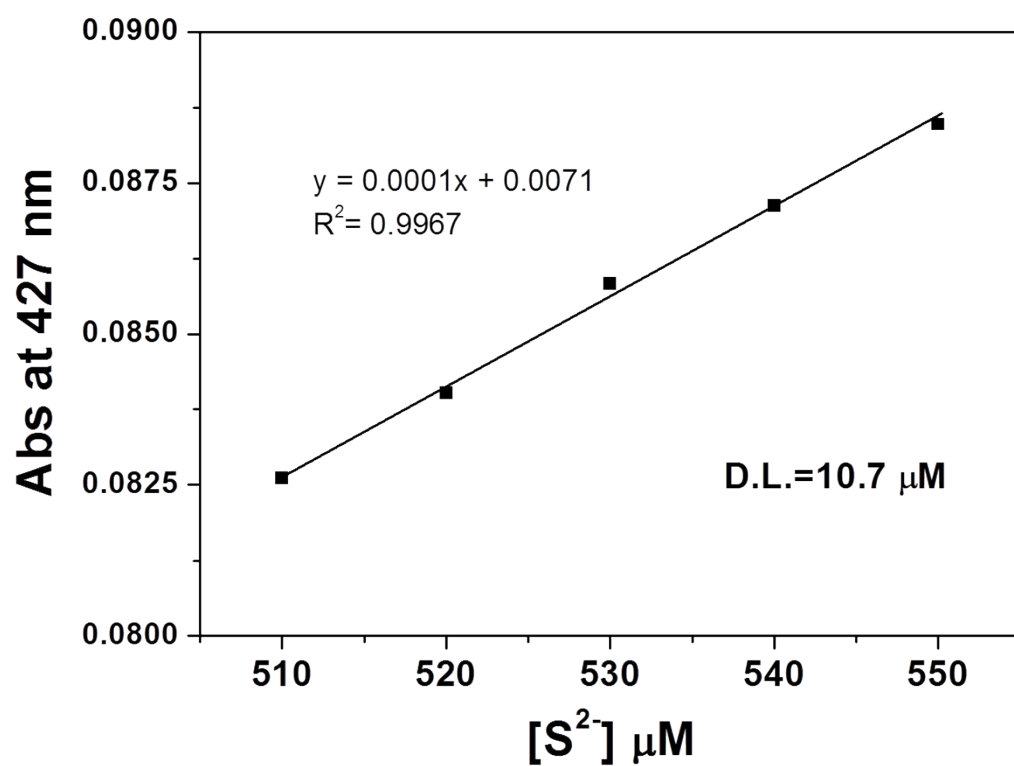
Figure S23. Determination of the detection limit based on change in the ratio (absorbance at 427 nm) of **1** (10 μM) with S^{2-}.
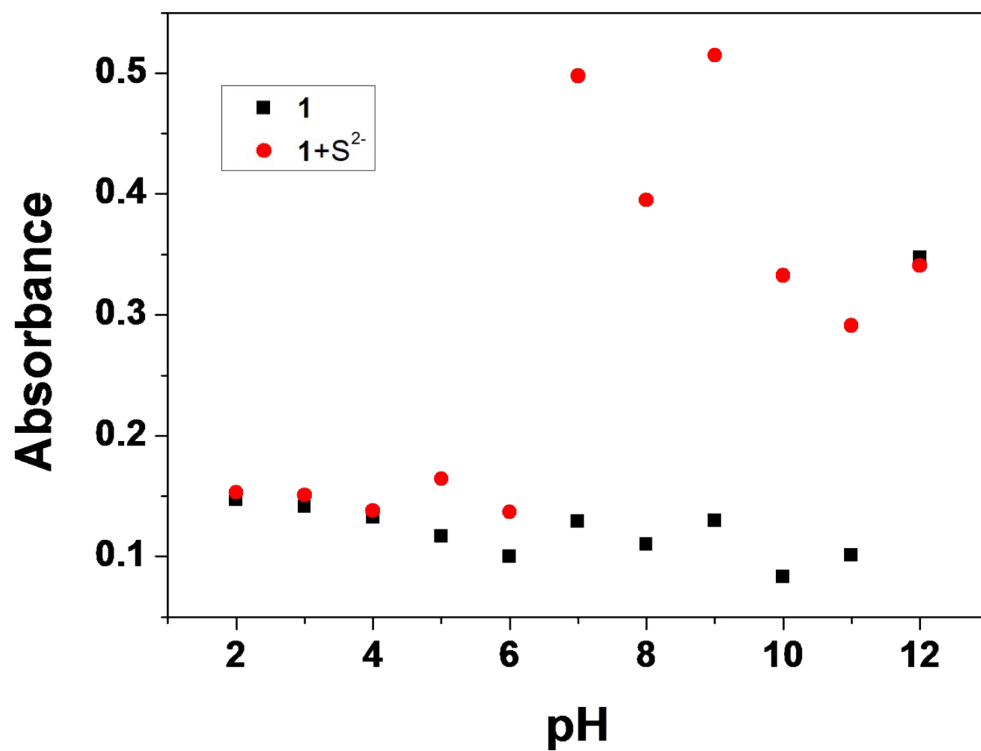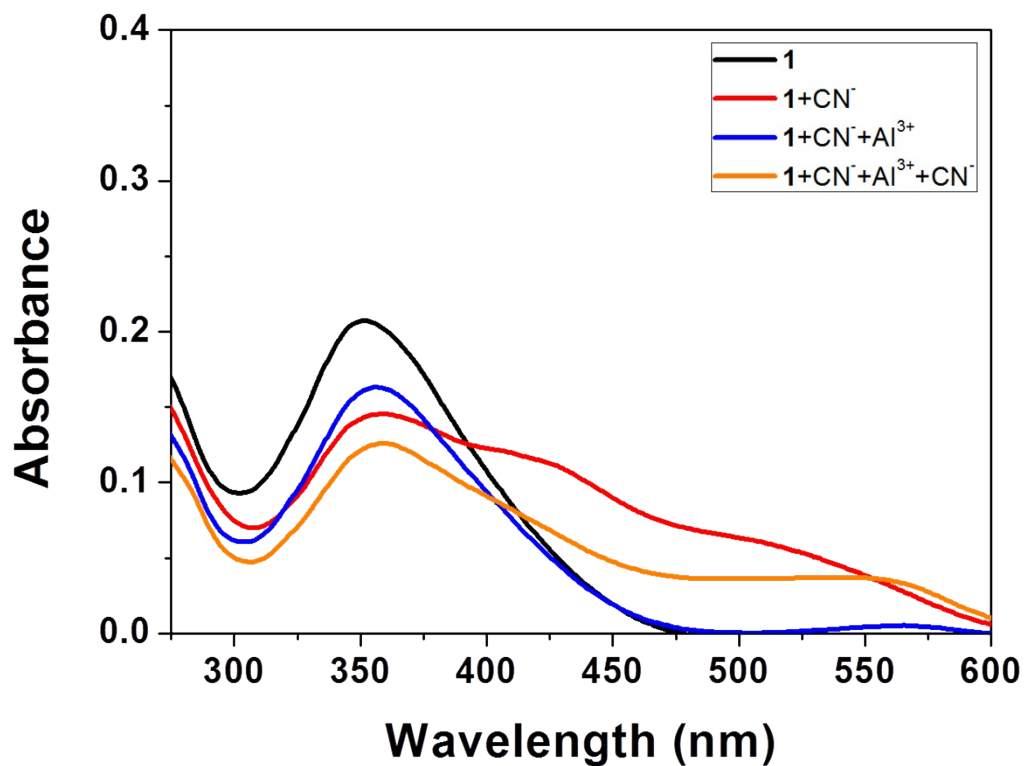
Figure S24. Absorbance (427 nm) of **1** and **1**-S^{2-} at different pH values (2-12) in a mixture of bis-tris buffer/DMSO (1:9, v/v).
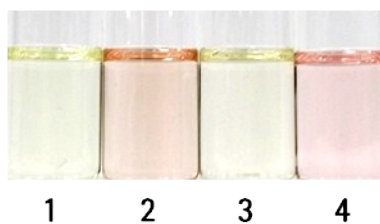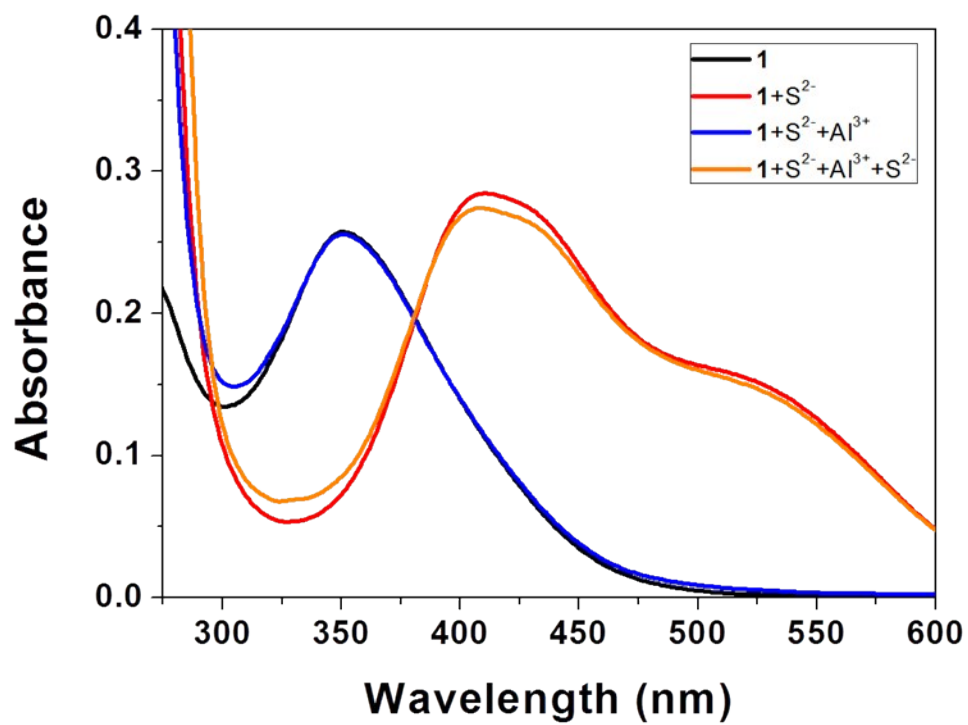
(a)

(b)

Figure S25. (a) Absorption spectra and (b) color changes of **1**, **1**-CN⁻, **1**-CN⁻ + Al³⁺ and **1**-CN⁻ + Al³⁺ + CN⁻ in a mixture of bis-tris buffer/DMSO (1:9, v/v). Conditions: **1** = 10 μM, CN⁻ = 260 equiv, and Al³⁺ = 30 equiv.

(a)

(b)

Figure S26. (a) Absorption spectra and (b) color changes of **1**, **1**-S^{2-}, **1**-S^{2-} + Al^{3+} and **1**-S^{2-} + Al^{3+} + S^{2-} in a mixture of bis-tris buffer/DMSO (1:9, v/v). Conditions: **1** = 10 μM, S^{2-} 88 equiv, and Al^{3+} 30 equiv.